ENG. Struct. Civ. Eng. 2026, 20(4): 706–720
https://doi.org/10.1007/s11709-026-1291-y

RESEARCH ARTICLE

Optimized silica fume replacement for enhanced early-age thermal cracking resistance in high-performance concrete: Experimental and numerical evaluation

Duy Tien NGUYEN[a], Tu Anh DO[a*], Viet Hai HOANG[a], Tuyet Thi HOANG[b], Duc Tam TRAN[c]

[a] *Faculty of Civil Engineering, University of Transport and Communications, Hanoi 100000, Vietnam*
[b] *Faculty of Basic Sciences, University of Transport and Communications, Hanoi 100000, Vietnam*
[c] *Faculty of Civil Engineering, VNU University of Engineering and Technology, Hanoi 100000, Vietnam*
[*] *Corresponding author. E-mail: doanhtu@utc.edu.vn*

ABSTRACT High-performance concrete (HPC) is increasingly being utilized in construction due to its improved qualities; however, its high cement content and low water-to-cement ratio cause significant heat generation during hydration, raising the danger of early-age thermal cracking. This study investigates the thermal cracking risk in HPC with varying levels of silica fume (SF) replacement (0%, 5%, 10%, and 15% by weight of cementitious materials). Experimental investigations were performed to determine the adiabatic temperature rise, compressive and cracking tensile strengths, and coefficient of thermal expansion of the four concrete mixtures. These experimental results were then used as input parameters for numerical simulations using the "EACTSA" program to assess temperature evolution, thermal stress development, and cracking potential in a representative bridge pier. The results indicate that while increasing SF content can accelerate early-age strength gain, its effect on thermal cracking risk is governed by the interaction between reduced thermal gradients and improved mechanical properties. SF replacement at 10% and 15% resulted in significantly lower cracking risk compared to 0% and 5%. This reduction reflects the combined effects of enhanced early-age tensile strength and reduced heat generation, with strength appearing more influential, although their relative contributions were not quantified and should be further investigated.

KEYWORDS HPC, SF, thermal stress, early-age thermal cracking, cracking potential

1 Introduction

High-performance concrete (HPC) has become increasingly popular in modern construction due to its superior mechanical properties and durability. However, its low water-to-cement (*w*/*cm*) ratio and high cement content result in significant heat generation during hydration, leading to steep thermal gradients within the concrete. This can cause early-age thermal cracking, compromising structural integrity and long-term performance [1,2]. Traditionally, research on the thermo-mechanical behavior of concrete has primarily focused on mass concrete elements, such as dams and large foundations, where heat accumulation occurs mainly within the core due to the slow dissipation of hydration heat. The resulting temperature differential between the core and surface induces thermal stresses that may exceed the concrete's tensile strength, leading to cracking [1–8]. However, with the widespread use of HPC, early-age thermal cracking is no longer limited to massive concrete structures. Even slender structural elements can experience significant temperature variations due to their dense microstructure and high cement content. As a result, the conventional definition of "mass concrete" has expanded beyond large concrete volumes to include thin-walled components susceptible to thermal cracking at early stages.

While early-age thermal cracking has traditionally been associated with mass concrete structures such as dams and large foundations, recent studies have shown that

Article history: Received Apr 16, 2025; Accepted Dec 2, 2025

slender elements can also be highly vulnerable. For example, Do et al. [9,10] investigated high-strength/HPC bridge elements, reporting heat of hydration, adiabatic temperature rise (ATR), and thermal stress development, and highlighted the risk of early-age cracking even in non-massive components. Do et al. [11,12] conducted finite element investigations on segmental box-girder diaphragms, demonstrating that slender bridge components are particularly susceptible to early-age thermal cracking when high-strength concrete or HPC is used. Extending this evidence, Li et al. [13] identified zero-stress and cracking temperatures of a thin HPC slab with external restraint, providing critical insight into tensile stress development at early ages. Ruano et al. [14] demonstrated that slender prestressed concrete beams are especially vulnerable to thermal strains and creep effects. Moreover, Phan et al. [15] confirmed through numerical simulations that reinforced concrete deck slabs in multi-span bridges exhibit early-age cracking risks under thermal and staged construction stresses. These findings indicate that the definition of "mass concrete" should be broadened to include not only massive blocks but also slender HPC elements such as bridge decks, diaphragms, and prestressed members, which can experience comparable risks of early-age thermal cracking. By integrating this perspective, the present study aims to bridge the gap between traditional mass concrete research and the emerging challenges in slender HPC elements.

Thermal cracking at an early age occurs when the tensile stresses induced by temperature gradients exceeds the developing tensile strength of hardening concrete (Fig. 1). Most existing mitigation strategies focus on reducing thermal gradients within concrete elements. However, to effectively prevent early-age cracking, it is also crucial to consider mechanical properties such as strength development and the evolution of elastic modulus. Notably, the enhancement of early-age tensile strength plays a pivotal role in minimizing crack formation.

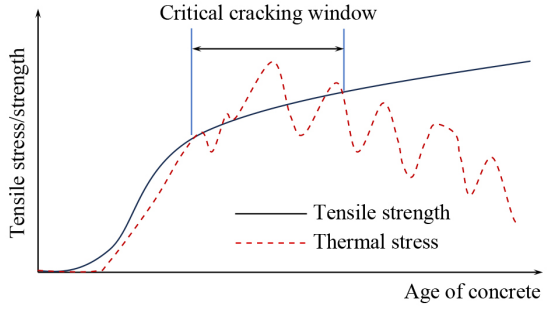

Fig. 1 Thermal stress and tensile strength development (adapted from Ref. [16] and based on authors' simulation results).

To address early-age thermal cracking, various supplementary cementitious materials (SCMs), such as ground granulated blast furnace slag (GGBFS or slag), fly ash (FA), and silica fume (SF), have been incorporated into concrete mixtures. While these SCMs help reduce hydration heat and modify mechanical properties, their influence on cracking risk is indirect, as it depends on the interplay between reduced thermal gradients and changes in tensile strength and stiffness. By partially replacing cement, SCMs lower the overall heat of hydration, thereby mitigating thermally induced stresses. However, while FA and GGBFS replacements are effective in reducing internal temperature rise, studies suggest that they can also delay strength development, leading to lower early-age compressive and tensile strengths, which may, in turn, compromise cracking resistance [16−18].

SF, a highly reactive pozzolanic material, has emerged as a promising admixture for improving both mechanical and thermal properties of concrete [19]. When incorporated into cementitious systems, SF enhances durability, impermeability, and mechanical strength, particularly at early ages. Unlike FA and GGBFS, which primarily influence long-term performance, SF contributes to the early-age development of compressive and tensile strength, thereby improving resistance to thermal cracking [19].

The presence of SF influences the hydration process by accelerating heat generation due to its pozzolanic reaction. The high surface area of SF enhances the hydration of alite, a principal component of Portland cement, resulting in increased early-age heat evolution [20]. Studies by Kurdowski and Nocuń-Wczelik [21] further confirmed that the initial hydration of alite is intensified in the presence of highly active silica. This suggests that Portland cement with high alite content can particularly benefit from SF incorporation.

Experimental data on the heat of hydration of SF-incorporated cement systems have been extensively studied. Cheng-yi and Feldman [22] used isothermal calorimetry to measure heat evolution in cement pastes containing 0%, 10%, 20%, and 30% SF. Their findings indicate that, although SF replacement increases the initial rate of heat release, the total cumulative heat per unit mass of solid material slightly decreases as SF content increases. Similarly, Kumar and Roy [23] reported that total heat liberation could be reduced by 15%–30%, depending on the specific cement type and SF dosage. Meland [24] also observed a reduction in total heat release for cement pastes incorporating 10% and 20% SF, which further supports the dilution effect of SF on overall heat production. Additionally, the studies indicate that SF concrete gains strength much faster than conventional concrete during early hydration stages.

Recent studies have provided extensive insights into the effectiveness of SF in improving concrete mechanical properties and mitigating thermal cracking. Shen [25] studied the influence of varying SF dosages on

temperature evolution, mechanical performance, and resistance to early-age cracking. The findings indicated that while higher SF content improved early mechanical strength, it also led to greater autogenous shrinkage and tensile creep under uniaxial restraint, ultimately diminishing the material's resistance to early-age cracking. Hamada et al. [26] showed that concrete flexural, tensile, and compressive strengths were influenced depending on the concentration of the SF. They also observed that SF refined the pore structure but increased drying shrinkage through its pozzolanic reaction. Singh and Singh [27] reported that incorporating SF at levels between 10% and 25% of the cement content enhanced the split tensile strength, compressive strength, and flexural strength of the mix. However, replacing more than 25% of the cement with SF negatively affected the overall performance of the composite.

Moreover, recent investigations have further highlighted the dual role of SF in both heat mitigation and strength enhancement, thus reducing thermal cracking risk. Shen et al. [28] demonstrated that different SF dosages reduced peak temperature rise and restrained thermal stresses, thereby lowering early-age cracking risk under restrained conditions. Xi et al. [29] confirmed that SF alters hydration kinetics in ultra-high-performance concrete, reducing the overall heat release rate while enhancing early-age strength development. Smarzewski [30] provided microstructural and mechanical evidence that SF reduces microcracking and improves fracture energy, supporting improved resistance against thermal stress. In addition, Peknikova et al. [31] observed that HPC mixtures incorporating SF retained higher compressive and flexural strengths, as well as improved durability indicators, compared to ordinary portland concrete after exposure to elevated temperatures, underscoring the superior thermal resilience of SF–HPC.

Concrete cracks when and where tensile stress exceeds tensile strength. Thus, enhancing tensile strength is critical for crack resistance. Tensile stress during the first few days after placement can be mitigated by reducing the modulus of elasticity; minimizing deformation due to temperature differentials and shrinkage; controlling the temperature of hardening concrete; or managing the temperature difference between new concrete and its foundation or previously cast elements. Overall, recent studies confirm that SF enhances early-age strength development and refines microstructure, while also influencing heat evolution and thermal stress. Yet, despite these advances, the literature does not clearly explain how these mechanisms combine to reduce early-age thermal cracking risk in HPC, particularly under restrained or slender structural configurations. To address this gap, the present study formulates and tests two hypotheses linking SF incorporation to thermal cracking resistance.

1) Hypothesis 1. Reduction in hydration heat: as SF replaces cement, the total heat released decreases, thereby reducing temperature differentials (ΔT) and lowering thermal stress development (Fig. 2(a)).

2) Hypothesis 2. Increase in early-age tensile strength: SF accelerates strength gain, enabling concrete to withstand early-age thermal stresses more effectively (Fig. 2(b)).

These two mechanisms may act simultaneously to improve the thermal cracking resistance of SF concrete, particularly in bridge structures where large temperature fluctuations occur during hydration. To test these hypotheses, this study combines experimental investigations of temperature evolution and strength development with numerical simulations of thermo-mechanical behavior to evaluate cracking risk.

This study aims to expand on this extensive research by evaluating the thermal cracking risk in HPC with varying levels of SF replacement. By integrating experimental analysis with advanced simulation techniques, this research seeks to provide a comprehensive understanding of proper mix designs that minimize early-age thermal cracking in HPC. The findings will contribute to the development of more durable and resilient concrete structures, particularly in bridge engineering applications where early-age cracking remains a critical concern.

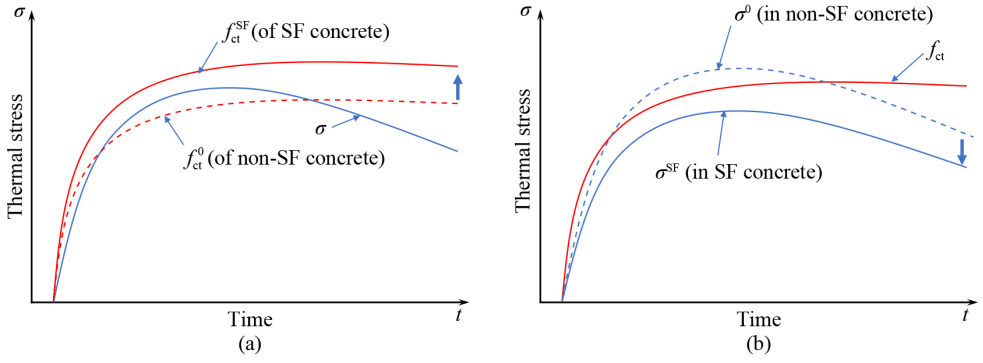

Fig. 2 Hypothesis on the trends that occurs when using SF replacement in concrete: (a) reduced thermal stress due to dilution effect; (b) increased strength of concrete due to SF.

2 Materials and methods

2.1 Materials

The chemical composition of the cement is detailed in Table 1. The coarse aggregate was made up of limestone with a maximum size of 12.5 mm.

SF was used as a mineral admixture in this study. Its chemical composition, provided by the manufacturer, is presented in Table 2. The material is characterized by a very high amorphous silica content (96.2%) and only minor amounts of carbon, Fe_2O_3, Al_2O_3, and other oxides (< 2%). Such composition, in line with the requirements of ASTM C1240-15 [32], indicates strong pozzolanic reactivity and suitability for improving early-age performance of HPC. A scanning electron microscope (SEM) image of the SF is shown in Fig. 3.

2.2 Mixture proportion

The mix design is presented in Table 3. In this study, concrete mixtures with different SF replacement levels, 0%, 5%, 10%, and 15% by weight of the cementitious materials, were prepared and designated as SF00, SF05, SF10, and SF15. The selected range of SF replacement was determined based on recommendations in ACI 211.4R-08 [33], which considers 0%–15% as practical for high-strength concrete and HPC. This choice is also consistent with Shen et al. [28], who evaluated SF at the same replacement levels. In addition, Smarzewski [30] suggested that SF substitution should not exceed 20%, while Singh and Singh [27] reported that replacement above 25% could negatively affect overall performance. On this basis, the 0%–15% range was adopted in the present study, with higher levels (e.g., 20%–25%) reserved for future investigation to further assess the potential of SF in HPC.

Table 1 Chemical composition of cement

Component	Percentage (%)
SiO_2	21.49
CaO	63.56
Al_2O_3	5.40
MgO	1.40
Fe_2O_3	3.49
SO_3	1.65
Na_2O	0.15
K_2O	0.70
Na_2O_{eq}	0.61

Table 2 Chemical composition of SF used in this study (manufacturer's data)

Component	Percentage (%)
SiO_2	96.2
C	< 2.0
Fe_2O_3	< 1.0
Al_2O_3	< 0.5
MgO, CaO, Na_2O, K_2O	< 0.5

2.3 Test of concrete strength

The compressive and splitting tensile strengths were measured on 0.15 m × 0.3 m cylindrical specimens made with four concrete mixtures at 1, 2, 3, 7, and 28 d. The compressive strength test was realized in accordance with ASTM C39 [34] while the splitting tensile strength test was performed following ASTM 496-04 [35]. The test results were then used to assess the development of compressive and splitting tensile strengths.

2.4 Test of adiabatic temperature rise

The concrete mixtures were tested to determine the ATR, which served as an input for the temperature prediction model in the following sections. ATR measurements were conducted using an adiabatic calorimeter developed based

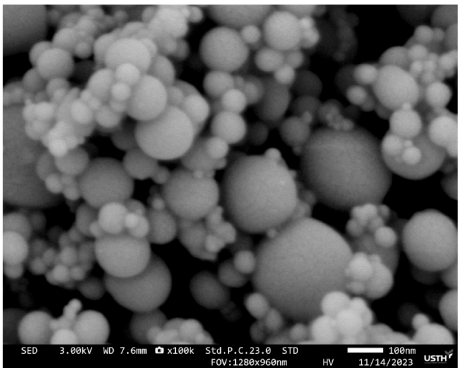

Fig. 3 SEM image of SF.

Table 3 Mix proportion of SF concrete

Mix	SF replacement	*w/c*	Water (L)	Cement (kg)	SF (kg)	Coarse aggregate (kg)	Sand (kg)	HRWR (kg)
SF00	0%	0.32	169	530	0	1098.2	620.4	5.5
SF05	5%	0.32	169	503.5	26.5	1098.2	611.8	5.5
SF10	10%	0.32	169	477	53	1098.2	603.2	5.5
SF15	15%	0.32	169	450.5	79.5	1098.2	594.6	5.5

Note: *w/c* = water to cementitious materials ratio; HRWR = High Range Water Reducing & Retarding admixture.

on the concept of Gibbon et al. [36] and further refined by Lin and Chen [4]. The apparatus is shown in Figs. 4(a) and 4(b), and the fresh concrete sample before testing is presented in Figs. 4(c) and 4(d).

In this system, heat exchange between the hydrating concrete and the surrounding environment was minimized by continuously matching the water temperature to the specimen temperature. The heating unit was automatically regulated by the calorimeter control system to maintain stable thermal conditions, with a measurement accuracy of ±0.1 °C. Thermal isolation was further enhanced by using a high-porosity foam layer instead of a conventional air gap, thereby achieving conditions closer to an ideal adiabatic state. Prior to testing, the calorimeter was calibrated to ensure accuracy, and repeated tests on identical paste samples were conducted to verify reproducibility. These measures ensured methodological reliability and confirmed the robustness of the calorimeter design.

During the process of hydration reactions, the rate of heat generation is influenced by the concrete temperature, with elevated temperatures accelerating the hydration reactions of cementitious materials. The degree of cement hydration is directly proportional to the amount of heat released, has been demonstrated in previous study [37], as expressed in Eq. (1):

$$\alpha(t) = \frac{H(t)}{H_u}, \tag{1}$$

where $\alpha(t)$ represents the degree of hydration, H_u is the total heat available for reaction (J/g) and $H(t)$ denotes the cumulative heat released by the cement (J/g), calculated based on the chemical composition using Eqs. (2) and (3):

$$H_u = H_{cem} p_{cem} + 461 p_{slag} + 1800 p_{FA} p_{FA-CaO}, \tag{2}$$

$$H_{cem} = 500 p_{C_3S} + 260 p_{C_2S} + 866 p_{C_3A} + 420 p_{C_4AF} + 624 p_{SO_3} + 1186 p_{FreeCa} + 850 p_{MgO}, \tag{3}$$

where H_{cem} is the total heat of hydration of the cement (J/g), p_{slag} is the percentage of slag in the cementitious materials, $p_{FA\text{-}CaO}$ is the percentage of CaO in the FA, p_{FA} represents the percentage of FA in the cementitious materials, p_X indicates the percentage of component X in the cement (X is component of cement such as C_3S, C_2S, C_3A, free Ca, MgO, C_4AF, or SO_3), and p_{Na2Oeq} refers to the sodium equivalent alkali content in the cement ($0.658 \times \%K_2O + \%Na_2O$).

A three-parameter mathematical model for the degree of hydration, presented in Eq. (4), has been employed to identify temperature development in concrete, as it accounts for the influence of temperature through the concept of equivalent age (Eq. (4)).

$$\alpha(t_e) = \alpha_u \exp\left(-\left[\frac{\tau}{t_e}\right]^{\beta}\right), \tag{4}$$

where α_u denotes the ultimate degree of hydration, τ and β are hydration model parameters, and t_e represents the equivalent age (or maturity) of the concrete in hours, as defined in Eq. (5):

$$t_e = \int_0^t \exp\left(\frac{E_a}{R}\left(\frac{1}{T_r} - \frac{1}{T_c(t)}\right)\right) dt, \tag{5}$$

where E_a is the apparent activation energy (J/mol), determined from the chemical composition using Eq. (6) [38], $T_c(t)$ is the temperature of the concrete (K), R is the universal gas constant (8.314 J/(mol·K)), and T_r is the reference temperature (K).

$$E_a = 41230 + 1416000(p_{C_3A} + p_{C_4AF}) p_{cem} p_{SO_3} p_{cem} - 347000 p_{Na_2O_{eq}} - 19.8 Blaine + 29600 p_{FA} p_{FA\text{-}CaO} + 16200 p_{slag} - 51600 p_{SF}, \tag{6}$$

where $p_{Na_2O_{eq}}$ refers to the sodium equivalent alkali content in the cement, p_{SF} is the percentage of SF in the cementitious materials, and Blaine is the fineness of the cement (m^2/kg).

To apply the hydration model in Eq. (4), the α_u, τ, and β parameters are obtained by fitting Eq. (4) to the calculated degree of hydration based on the measured

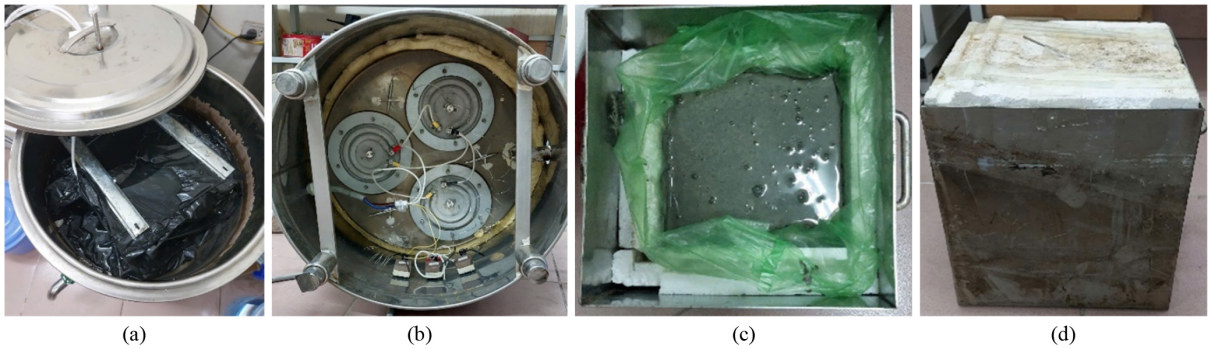

(a) (b) (c) (d)

Fig. 4 Experimental setup for adiabatic temperature test: (a) adiabatic calorimeter; (b) heater located at the bottom of the tank/chamber; (c) fresh concrete sample; (d) and sample container to be placed in the tank.

ATR. The cumulative heat of hydration, which is used in Eq. (2) to compute the degree of hydration, can be derived from Eq. (7):

$$H(t) = \frac{m_s}{m_{cm}} c_p T(t), \tag{7}$$

where m_s is the mass of the concrete test sample, m_{cm} is the mass of the cementitious materials in the sample, and $T(t)$ represents the experimentally measured ATR.

The cumulative heat released, $Q(t_e)$, can be calculated from the degree of hydration, $\alpha(t_e)$ as outlined in Eq. (8). The heat rate can subsequently be computed using Eqs. (9) and (10).

$$Q(t_e) = Q_c \cdot \alpha(t_e), \tag{8}$$

$$q(t_e) = \frac{dQ}{dt_e} = Q_c \cdot \alpha(t_e) \cdot \left(\frac{\tau}{t_e}\right)^{\beta} \cdot \frac{\beta}{t_e}, \tag{9}$$

$$q(t) = \frac{dQ}{dt} = \frac{dQ}{dt_e} \cdot \frac{dt_e}{dt} = Q_c \cdot \alpha(t_e) \cdot \left(\frac{\tau}{t_e}\right)^{\beta} \cdot \frac{\beta}{t_e} \cdot \exp\left(\frac{E_a}{R}\left(\frac{1}{T_r} - \frac{1}{T_c(t)}\right)\right), \tag{10}$$

where Q_c represents the total available heat per unit volume (J/m^3).

2.5 Coefficient of thermal expansion measurement

Under saturated conditions, the coefficient of thermal expansion (CTE) is determined by monitoring length changes of cylindrical concrete specimens in response to controlled temperature variations, in accordance with the AASHTO T336 standard [39]. The test starts at 10 °C, gradually increasing to 50 °C, stabilizing, and then decreasing back to 10 °C. This process is repeated multiple times to ensure reliable data. Each concrete mix is tested using two cylindrical specimens with a nominal diameter of 100 mm and a length of (177.8 ± 2.54) mm. The system used for measuring the CTE of the specimens is shown in Fig. 5.

3 Results and discussion

3.1 Early strength development

The compressive strengths of SF concrete mixtures at various ages are provided in Table 4 and showed in Fig. 6, while the splitting tensile strengths are shown in Table 5 and depicted in Fig. 7.

At 1 d of age, the concrete mixtures achieved more than 50% of their 28-d compressive strength, and by 3 d, their compressive strength exceeded 75% of the 28-d value. Notably, the SF-containing mixtures (SF05, SF10, and SF15) surpassed 80% of the 28-d compressive strength at 7 d. This highlights the considerable benefit of SF concrete mixtures in attaining high early-age compressive strength, making them ideal for bridge structural components that require early prestressing within 3 d.

At 1 d of age, the concrete mixtures attained a splitting tensile strength greater than 65% of their 28-d value. By

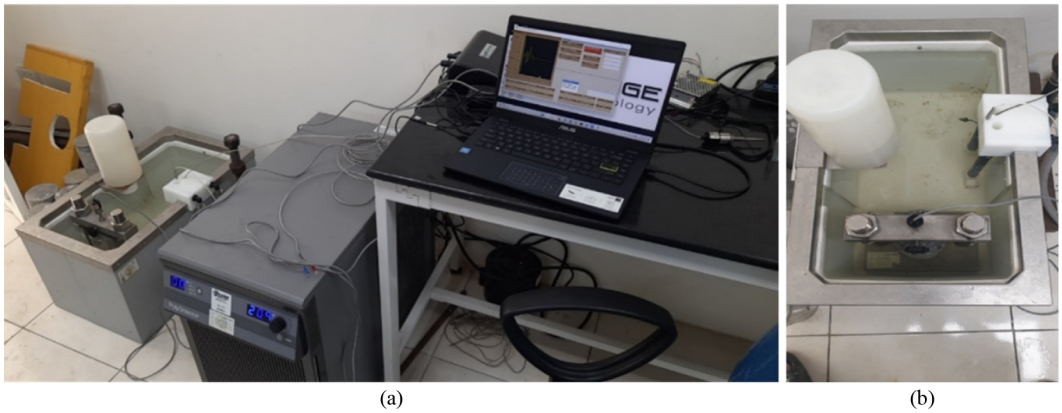

(a) (b)

Fig. 5 CTE measurement system: (a) overview of the system; (b) water tank containing the concrete sample.

Table 4 Compressive strength (MPa)

Age (d)	SF00	SF05	SF10	SF15
1	38.54	39.26	39.13	41.24
2	49.02	50.53	50.72	50.23
3	51.23	53.52	55.80	56.62
7	52.45	60.44	61.03	62.63
28	66.26	69.06	73.34	71.65

Table 5 Splitting tensile strength (MPa)

Age (d)	SF00	SF05	SF10	SF15
1	3.21	3.78	3.54	3.78
2	3.75	4.04	4.22	4.32
3	4.15	4.34	4.29	4.45
7	4.27	4.49	4.80	4.56
28	4.70	4.89	5.13	5.07

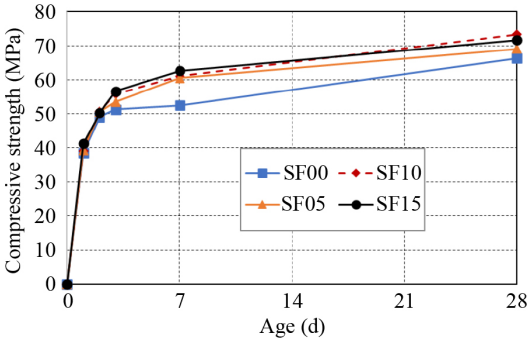

Fig. 6 Development of compressive strength of SF concrete mixtures (MPa).

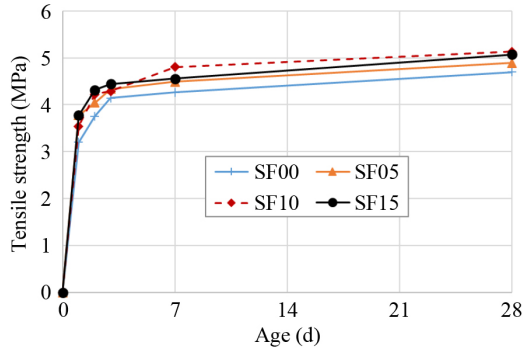

Fig. 7 Development of tensile strength of SF concrete mixtures (MPa).

3 d, the tensile strength exceeded 80% of the 28-d value. This demonstrates that SF concrete mixtures provide notable benefits in improving early-age tensile strength and resistance to thermal cracking.

The mechanistic basis for these improvements lies in the pozzolanic reactivity of SF. In addition to a filler effect that refines the particle packing, SF rapidly consumes calcium hydroxide released during cement hydration, forming additional C–S–H gel, which strengthens the microstructure and accelerates strength development at early ages [26,29]. Hamada et al. [26] further highlighted that SF contributes to densification through both chemical and physical effects, while Shen [25] emphasized its role in improving cracking resistance by increasing early tensile capacity. These combined mechanisms explain why mixtures with 5%–10% SF exhibited higher strength compared to plain concrete, while performance gains leveled at 15% replacement due to dilution effects.

Schutter [40] confirmed that the early-age compressive strength (f_c) and tensile strength (f_{ct}) of early mixture are generally related to the degree of cement hydration (α). This correlation has also been verified and confirmed by the research of Lin and Chen [18]. Schutter [40] and Fairbairn [41] presented this correlation in the form of Eqs. (11) and (12).

$$f_c(t) = [\alpha(t)]^a f_c,\ (\alpha = 1)(\text{MPa}), \tag{11}$$

$$f_{ct}(t) = [\alpha(t)]^b f_{ct},\ (\alpha = 1)(\text{MPa}), \tag{12}$$

where α is the degree of hydration, a and b are coefficients determined from the regression curve of the experimental data (a ranging from 0.84 to 1.4, and b ranging from 0.46 to 0.88 [40]), $f_c(t)$ and $f_{ct}(t)$ are compressive strength and tensile strength over time, respectively, $f_c(\alpha = 1)$ and $f_{ct}(\alpha = 1)$ are compressive strength and tensile strength, respectively, at the end of the hydration process, assuming $\alpha = 1$. However, in practice, when considering early age concrete within 7 d, the endpoint can be approximated as 7 d. In that case, the coefficients should be adjusted accordingly using the following relationships:

$$f_c(t) = p_c[\alpha(t)]^a, \tag{13}$$

$$f_{ct}(t) = p_{ct}[\alpha(t)]^b, \tag{14}$$

where p_c, p_{ct} are coefficients determined from the regression curve of the experimental data. Model parameters for strength development are presented in Table 6.

Table 6 Model parameters for strength development

Mixture	p_c (MPa)	a	p_{ct} (MPa)	b
SF00	75.72	0.6273	5.923	0.5899
SF05	92.83	0.8546	5.311	0.3428
SF10	113.00	1.1840	6.981	0.7595
SF15	150.00	1.8630	6.901	0.8460

The elastic modulus of concrete is calculated according to ACI 209.2R-08 [42]:

$$E_c(t) = E_{cm28}\left(\frac{t}{4 + 0.85t}\right)^{0.5}(\text{MPa}), \tag{15}$$

where $E_c(t)$ is the elastic modulus of concrete (MPa) at the age of t (d), E_{cm28} denotes the elastic modulus of concrete (MPa) at the age of 28 d, which can be calculated based on the compressive strength of concrete aging 28 d as follows [42]:

$$E_{cm28} = 4734\sqrt{f_{cm28}}(\text{MPa}), \tag{16}$$

where f_{cm28} is the mean 28-d compressive concrete strength.

3.2 Effect of silica fume on adiabatic temperature rise

The measured ATR of the concrete mixtures is presented in Fig. 8(a). The initial temperatures of the SF00, SF05, SF10, and SF15 samples were 24.1, 29.7, 27.4, and 28.0 °C, respectively. The maximum temperatures recorded at the end of the experiment were 80.2, 84.6,

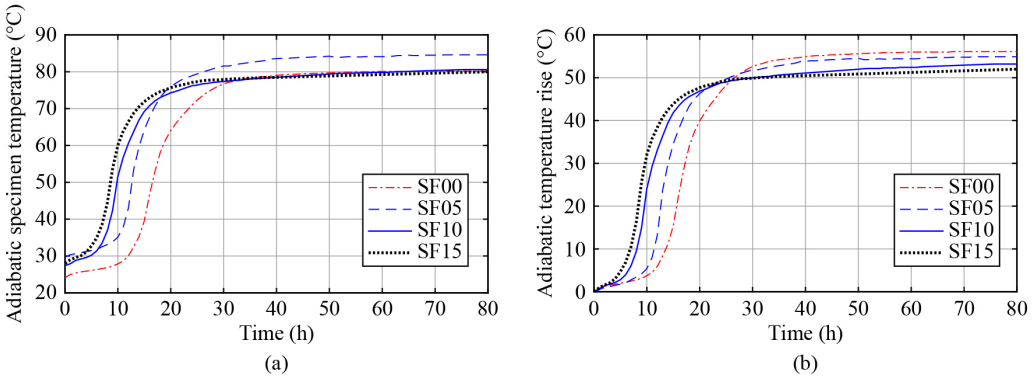

Fig. 8 Effect of silica fume on adiabatic temperature: (a) measured adiabatic specimen temperatures and; (b) ATRs of 4 mixtures.

80.6, and 80.0 °C, respectively. To evaluate the ATR, the measured temperature of each sample was subtracted from its initial temperature, as shown in Fig. 8(b). The maximum ATR values for SF00, SF05, SF10, and SF15 were 56.1, 54.9, 53.2, and 52.0 °C, respectively. As expected, the heat released increases with a higher cement content in the mixture.

Due to its large surface area, increasing the SF content in concrete requires a higher dosage of superplasticizer (with a constant water content) to achieve the desired workability. However, in this study, to monitor and compare the heat development and strength of SF mixtures under the same dosage conditions, the same amount of superplasticizer was used for all four mixtures. As shown in Fig. 8, increasing the SF content accelerates the cement hydration reaction and leads to earlier heat development. This effect can be attributed to the presence of SF particles, which are much finer than cement particles and enhance the dispersion of cement grains. Consequently, the cement particles interact with water more quickly and in greater quantity, resulting in a faster hydration reaction in mixtures with higher SF content.

Nevertheless, despite this acceleration effect at early ages, the overall ATR of SF mixtures was lower than that of the plain mixture. This apparent contradiction can be explained by two concurrent mechanisms: 1) the nucleation effect of SF, which accelerates hydration and causes faster early heat evolution, and 2) the dilution effect, which reduces the total cement content and thus decreases the cumulative heat release. In the long-term, the dilution effect dominates, resulting in a lower ATR for SF concretes, even though their early-age reaction rate is faster. This dual mechanism reconciles the observed higher early strength with the reduced ATR of SF concretes, consistent with the findings of Xi et al. [29] and Hamada et al. [26].

3.3 Effect of silica fume on degree of hydration

The calculated activation energy (E_a) and the total heat available (H_u, Q_c) are provided in Table 7. The hydration parameters (α_u, τ, and β) were calculated by fitting Eq. (4) to the experimental data using the least-squares method, with these parameters also listed in Table 7. Figure 9 shows the experimental curve of degree of hydration for the four concrete mixtures alongside the corresponding fitted curves.

The relationship between the ultimate hydration degree (α_u) (Table 6) and the replacement percentage of SF is illustrated in Fig. 10. It can be observed that the ultimate hydration degree almost linearly increases with the SF replacement percentage. Note that Schindler and Folliard [37] has addressed the influence of FA and/or slag on the ultimate hydration degree as expressed in Eq. (17):

$$\alpha_u = \frac{1.031 \cdot w/cm}{0.194 + w/cm} + 0.5 \cdot p_{FA} + 0.3 \cdot p_{slag}. \quad (17)$$

where w/cm is the water to cement ratio. While previous studies have examined the effects of FA and slag on the ultimate hydration degree, the influence of SF has not been explicitly investigated. Given that the concrete mixtures in this study incorporate SF but exclude FA and slag, Eq. (17) has been modified to account for the presence of SF, as proposed by the authors:

$$\alpha_u = \frac{1.031 \cdot w/cm}{0.194 + w/cm} + k_{SF} \cdot p_{SF}, \quad (18)$$

Table 7 Heat of hydration parameters for SF concrete mixtures

Mixture	τ (h)	β	α_u	H_u (J/g)	Q_c (J/m^3)	E_a (J/mol)	ρ (kg/m^3)	c_p (J/(kg·°C))
SF00	21.20	1.554	0.5839	459.731	2.43×10^8	36011	2424	1043
SF05	20.52	1.59	0.5953	436.744	2.31×10^8	33009	2416	1043
SF10	13.65	1.403	0.6037	413.758	2.19×10^8	30029	2407	1043
SF15	11.56	1.561	0.6208	390.771	2.07×10^8	27071	2398	1043

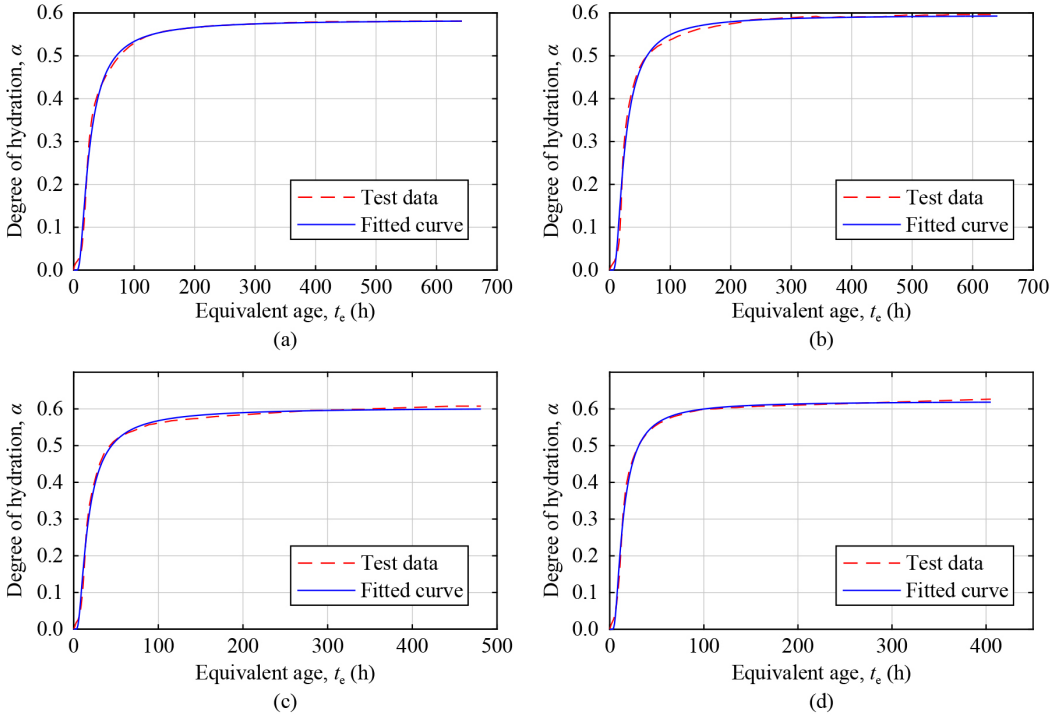

Fig. 9 Curves fitted for the degree of hydration: (a) degree of hydration for SF00; (b) degree of hydration for SF05; (c) degree of hydration for SF10; (d) degree of hydration for SF15.

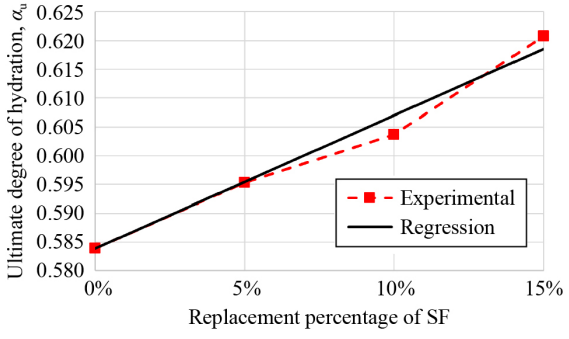

Fig. 10 Correlation between the ultimate degree of hydration and SF replacement percentage.

where k_{SF} is the regression coefficient determined using regression analysis.

A linear regression equation was determined using the least squares method, correlating the ultimate degree of hydration with the theoretical linear trend as follows (with the coefficient of determination R^2 of 0.9779):

$$\alpha_u = \alpha_{u,0} + k_{SF} \cdot p_{SF} = \alpha_{u,0} + 0.23 p_{SF}, \quad (19)$$

where $\alpha_{u,0}$ is the ultimate degree of hydration of SF00 (containing 100% cement), and k_{SF} is the regression coefficient, equal to 0.23.

It can be observed from Fig. 10 that the ultimate hydration degree tends to increase as the SF replacement level increases. This trend is consistent with previous findings on cement replacement with FA or slag, as reported by Schindler and Folliard [37]. However, the regression coefficient differs.

3.4 Coefficient of thermal expansion of silica fume concrete

Table 8 shows the CTE values for the four SF concrete mixtures obtained from experimental measurements. The CTE values ranged from 8.95 × 10^{-6} to 9.93 × 10^{-6} °C^{-1}, with modest variations among the mixtures. The effect of SF content on CTE is minimal, which is consistent with prior research showing that CTE is predominantly controlled by the type and volume fraction of coarse aggregate—which present a much larger amount of content [43]. While SF itself has a very low CTE compared to concrete, its influence in mixtures is mainly indirect, by refining the microstructure of the cement paste and densifying the interfacial transition zone. This can improve aggregate–paste bonding and reduce micro-cracking, slightly modifying how thermal strains are transferred. However, this secondary effect remains small compared to the dominant contribution of coarse aggregate volume and type, which explains the absence of a consistent trend in our results.

Table 8 CTE of SF concrete mixtures

Mixture	CTE (× 10^{-6} °C^{-1})
SF00	8.95
SF05	9.25
SF10	9.22
SF15	9.93

These CTE values are important physical properties of concrete and serve as input parameters for thermal stress analysis and the assessment of cracking risk induced by both internal and external temperatures at an early age, as provided in Section 4. Since this study did not measure the CTE of concrete at early ages (within the first few hours or few days after mixing), the measured CTE values presented here will be assumed constant over time for the analysis in the following sections.

4 Temperature development and early-age thermal cracking analysis

The experimental results in previous sections indicate that for SF concrete mixtures, increasing the SF replacement level slightly reduces the total accumulated heat, but enhances early-age strength. To evaluate the impact of SF content on temperature development, thermal stress, and the risk of early-age thermal cracking, a detailed and quantitative analysis is required. To achieve this, this section compares the temperature evolution, strength development, thermal stress, and cracking potential of a bridge pier with the same cross-section but made from the 4 different SF concrete mixtures. The analyzed bridge pier has typical dimensions used in bridge construction, with a cross-section of 2.8 m × 3.5 m. Since the bridge pier has a relatively greater height compared to its cross-sectional dimensions, a two-dimensional cross-sectional simulation at the mid-height of the structure is considered.

Numerical methods such as the finite element method, finite difference method, and Smoothed Particle Hydrodynamics [44] are powerful tools for thermo-mechanical analysis, enabling the simulation of temperature evolution, stress, and strain during the forming processes of structural materials. Building on these approaches, the present study employs the "EACTSA" (early-age concrete thermal stress analysis [45]) program to analyze temperature development and thermal stress in bridge piers. The EACTSA program, a hybrid finite element-finite difference model, was developed in MATLAB and its validation was established in prior research [18,45]. Specifically, the temperature and predicted stress profiles agree closely with ABAQUS finite element simulations and experimental measurements from large concrete cubes reported by Lin and Chen [18]. Therefore, the use of EACTSA in this study provides reliable estimates of early-age temperature and stress development. There are two processes to calculating early-age stress: temperature and stress analyses. The time-history-temperature distribution within the concrete section is then used as input loading for the stress analysis, in which EACTSA examines the change of material characteristics and the effects of creep at each time increment of 1 h.

Early-age concrete stress development is a complicated process that is influenced by temperature gradients as well as the concrete's elastic modulus, CTE, shrinkage, creep, and constraint circumstances [46]. The creep parameters of the Bazant-Baweja B3 model are determined according to ACI 209.2R-08 [42] for concrete mixtures, as shown in Table 9. These parameters are crucial for the thermal and mechanical behavior of early-age concrete. They will be incorporated into the EACTSA calculation program [45] for analysis.

Table 9 Creep parameters for SF mixtures

Item	q_1 ($\times 10^{-5}$ MPa^{-1})	q_2 ($\times 10^{-5}$ MPa^{-1})	q_3 ($\times 10^{-7}$ MPa^{-1})	q_4 ($\times 10^{-6}$ MPa^{-1})
SF00	1.614	10.460	3.210	8.910
SF05	1.525	9.200	3.467	8.626
SF10	1.480	8.483	3.969	8.335
SF15	1.497	8.419	4.951	8.036

It is noted that, in this study, the measured CTE values (Table 8) were assumed constant over time. While this assumption simplifies the modeling, it may not fully capture the behavior of early-age concrete, since hydration, porosity reduction, and moisture redistribution can cause slight variations in CTE, especially during the first 24 h after casting. Measuring these variations is challenging, as the thermal expansion response is strongly coupled with temperature and concrete maturity. For this reason, the thermal expansion coefficient is often assumed to be constant for simplicity, as also noted by Lin and Chen [18]. Given the lack of early-age CTE measurements in this work, the use of constant CTE values provides a reasonable and practical approximation for input to thermal stress analysis.

Other parameters used in the calculations are as follows: the initial concrete temperature is assumed to be 27 °C, the ambient temperature is based on actual measured values and therefore varies cyclically between day and night, and the surface convection coefficient with the ambient air is taken as h_c = 13.9 W/(m^2·K) [45,47,48].

Figure 11(a) shows the anticipated temperature histories in the center, mid-side, bottom, and corners of the concrete section using SF00. After 55–60 h of concrete pouring, the maximum temperature at the middle of the cross-section reaches 81.5 °C. Because of the massive concrete mass, the temperature of the core gradually declines after this peak. The temperature contour distribution across the pier cross-section at 55 h is illustrated in Fig. 11(b).

From the temperature profiles, the thermal stresses at different points over time are calculated using the EACTSA [45] program. Figure 12(a) illustrates that the section's mid-side has the greatest primary tensile stress. Thus, as illustrated in Fig. 12(b), the stress at this location is used to compare with the development of tensile strength.

From Fig. 12(b), it can be seen that the thermal stress curve goes higher than the tensile strength curve at 57 h, indicating a high risk of thermal cracking. Notably, after 70 h, the thermal stress decreases corresponding to a reduction in the temperature difference between the core and surface of the concrete.

The analyses for SF05, SF10, and SF15 are similar. Using SF05, SF10, and SF15, the temperature histories, maximum tensile stress, and tensile strength of the section are plotted in Figs. 13−15, respectively.

When examining the concrete's development curves for thermal stress and tensile strength over time for each of the four scenarios, it is evident that using SF10 and SF15 mixtures results in a tensile stress curve that stays below the tensile splitting strength curve for the entire seven-day period, suggesting a low risk of thermal cracking. The heat stress for SF00 and SF05 mixes, on the other hand, surpasses the tensile splitting strength for roughly 48 to 90 h (2–4 d).

To reduce the chance of cracking and/or manage the spread of cracks, it is crucial to predict the creation of thermal cracks in early-age concrete. The ratio of the

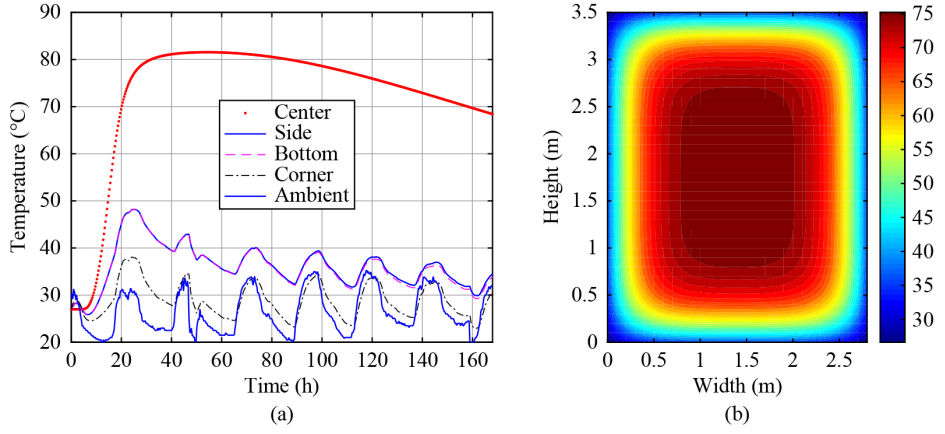

Fig. 11 Temperature development in the section using SF00: (a) temperature histories and (b) temperature contours.

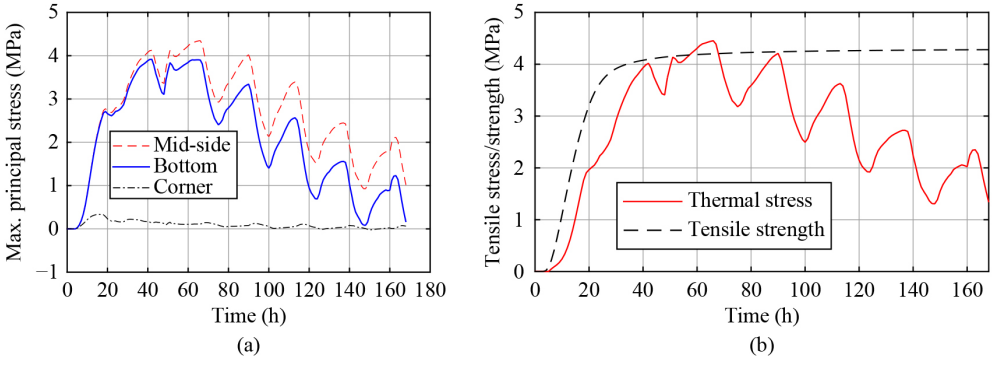

Fig. 12 Thermal stresses in the section using SF00: (a) principal stresses and (b) maximum tensile stress and tensile strength.

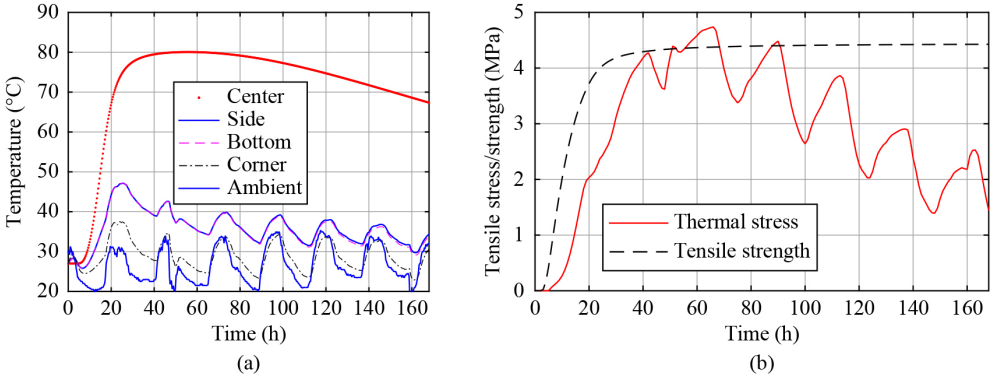

Fig. 13 Temperature histories, maximum tensile stress and tensile strength in the section using SF05: (a) temperature histories (b) stress/strength.

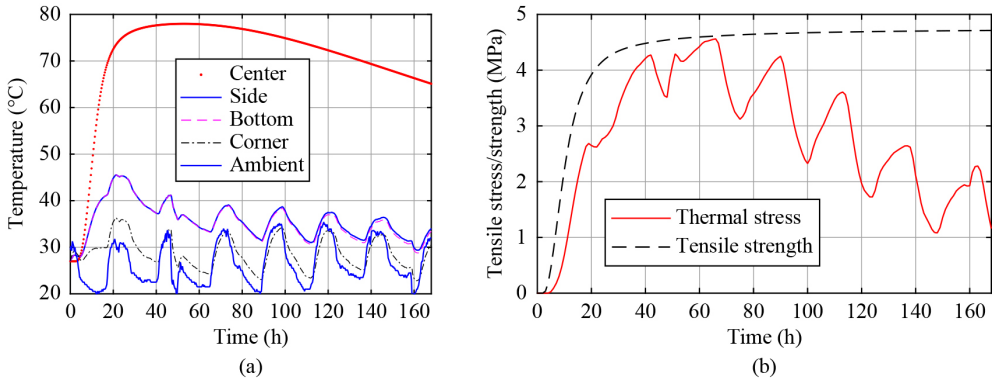

Fig. 14 Temperature histories, maximum tensile stress and tensile strength in the section using SF10: (a) temperature histories; (b) stress/strength.

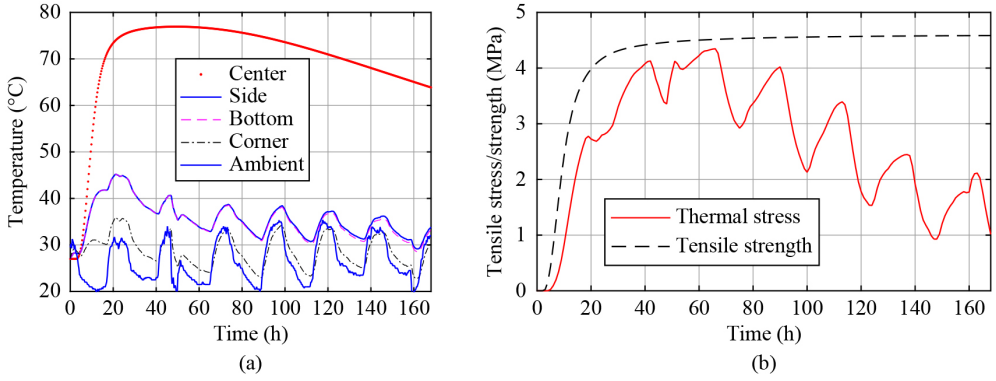

Fig. 15 Temperature histories, maximum tensile stress and tensile strength in the section using SF15: (a) temperature histories; (b) stress/strength.

concrete's splitting tensile strength with time to its thermal stress is used to calculate the thermal cracking potential, or risk, for any concrete mixture. This ratio is commonly defined as the cracking potential (η), as expressed in the following equation [49–52].

$$\eta(t) = \frac{\sigma(t)}{f_{ct}(t)}, \tag{20}$$

where η is the cracking potential, σ is the principal tensile thermal stress, f_{ct} is the tensile strength of concrete at the considered, t is time in hours.

It is important to note that temperature varies at different locations across the section, resulting in different equivalent ages (also referred to as maturity) of the concrete. Consequently, the strength development differs at every point. The cracking potential η provides a quick assessment of the cracking potential at a given point: if $\eta \geqslant 1$, cracking is most likely to occur; if $\eta < 1$, the concrete has a low risk of cracking or remains uncracked [50,51].

The maximum cracking potential η (at the critical location on the concrete section) is calculated for the 4 different concrete mixtures and presented in Fig. 16. It can be observed that for SF00 and SF05, η values exceed 1.0 during the period from 48 to 90 h (2–4 d), whereas for

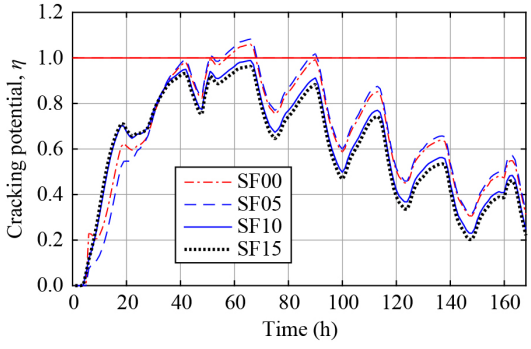

Fig. 16 Maximum η for SF concrete mixtures.

SF10 and SF15, η values remain below 1.0 throughout the first 7 d. This indicates that using SF10 and SF15 can reduce the risk of early-age thermal cracking compared to SF00 and SF05 under the same structural dimensions and ambient temperature conditions.

The maximum temperature differential (ΔT) between the core and the surface (mid-side of the section) for each concrete mixture is presented in Fig. 17. The ΔT values at the time the maximum η occurs (t = 66 h) for SF00, SF05, SF10, and SF15 are 46.86, 45.68, 44.43, and 43.67 °C, respectively, corresponding to the thermal stresses of 4.45, 4.74, 4.56, and 4.35 MPa, respectively (see Table 10).

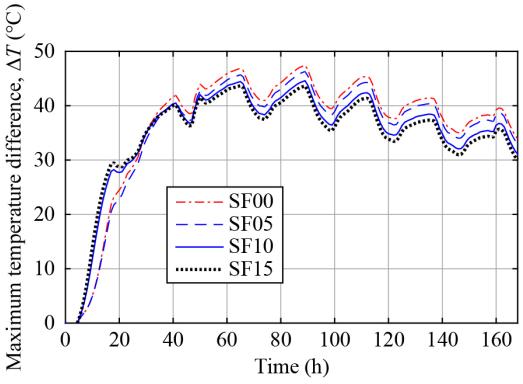

Fig. 17 Maximum temperature difference between the core and surface for SF concrete mixtures.

Notably, SF00 and SF05, which have the highest ΔT values, also exhibit the largest cracking potential (η = 1.0599 and 1.0827, respectively), compared to the cases of SF10 and SF15 (η = 0.9888 and 0.9628, respectively). This suggests that although SF concrete mixtures have significant internal heat, their rapid early-age strength development enhances their crack resistance. For SF10 and SF15, despite ΔT values reaching 43–44 °C, thermal cracking is unlikely.

Interestingly, while the ΔT value for SF05 is lower than that of SF00, the thermal stress in the SF05 case is actually higher. This can be explained by the fact that SF05 has a higher compressive strength than SF00, leading to a higher elastic modulus (Eqs. (15) and (16)). Consequently, the thermal stress also increases. This is not solely a function of ΔT, but rather the combined influence of thermal loading and evolving material properties. The partial replacement of cement with 5% SF accelerates hydration (compared to 0% SF), leading to a faster increase in compressive strength and, consequently, a higher modulus of elasticity (see Eqs. (15) and (16)). While this early stiffness gain is beneficial for load-bearing capacity, it simultaneously reduces the ability of the material to relax stresses through creep at early ages [42]. As a result, although the thermal gradient is slightly smaller in SF05, the reduced stress relaxation capacity leads to a higher net thermal stress compared with SF00. This highlights that restraint-induced stresses are governed by the balance between ΔT, stiffness growth, and creep compliance, rather than temperature rise alone.

To assess whether the "cement dilution effect due to SF replacement" in reducing the heat of hydration or the enhancement of splitting tensile strength from SF addition plays a more dominant role in mitigating thermal cracking risk, this study compares the variations in thermal stress (σ), temperature differential (ΔT), and cracking potential (η) across the 4 cases above. The changes in these parameters are evaluated using the following equations:

$$\%\sigma = \frac{\sigma - \sigma_{SF00}}{\sigma_{SF00}}, \tag{21}$$

$$\%\eta = \frac{\eta - \eta_{SF00}}{\eta_{SF00}}, \tag{22}$$

$$\%\Delta T = \frac{\Delta T - \Delta T_{SF00}}{\Delta T_{SF00}}, \tag{23}$$

where the subscript "SF00" indicates the parameter calculated for the SF00 mixture.

Table 10 presents the variations in thermal stress (σ), temperature differential (ΔT), and cracking potential (η) for SF05, SF10, and SF15 relative to SF00. The 'dilution effect' is evident in the reduction of ΔT as the SF replacement level increases. However, thermal stress and cracking potential do not exhibit the same trend. Specifically:

1) with 5% SF replacement, thermal stress increases by 6.5%, and the cracking potential rises by 2.2%;

2) with 10% SF replacement, thermal stress increases by 2.5%, but the cracking potential decreases by 6.7%;

3) with 15% SF replacement, thermal stress decreases by 2.2%, and the cracking potential drops by 9.2%.

Notably, when using 5% SF, despite the decrease in ΔT, both thermal stress and thermal cracking risk are higher than the case of SF00. In contrast, with 10% and 15% SF replacement, ΔT decreases by 5.2% and 6.8%, respectively, compared to SF00—corresponding to reductions of 6.7% and 9.2%, respectively, in the cracking potential η. These findings suggest that the enhancement in tensile strength due to SF addition plays a more dominant role in reducing thermal cracking risk than the reduction in hydration heat caused by the "cement dilution effect due to SF replacement."

Another important observation is that the time at which the maximum thermal cracking potential occurs does not necessarily coincide with the peak ΔT. As shown in Table 11, the maximum ΔT values of 47.44, 46.30, and 44.59 °C occur at 90 h after casting for SF00, SF05, and SF10, respectively. However, for SF15, the maximum ΔT

Table 10 Temperature difference between the core and surface corresponding to maximum η

Mixture	Max η	σ (MPa)	t (h)	T core (°C)	ΔT (°C)	σ (%)	η (%)	ΔT (%)
SF00	1.0599	4.45	66	81.3	46.86	–	–	–
SF05	1.0827	4.74	66	79.9	45.68	+6.5%	+2.2%	−2.5%
SF10	0.9888	4.56	66	77.7	44.43	+2.5%	−6.7%	−5.2%
SF15	0.9628	4.35	66	76.5	43.67	−2.2%	−9.2%	−6.8%

Table 11 Maximum temperature difference (ΔT max) between core and surface

Mixture	Max ΔT (°C)	Max T core (°C)	t (h)	η
SF00	47.44	79.7	90	0.9929
SF05	46.30	78.3	90	1.0185
SF10	44.59	75.9	90	0.9123
SF15	43.67	74.7	66	0.9628

occurs earlier, at 66 h, coinciding with the time of maximum η.

5 Conclusions

This study examined the influence of SF replacement on the thermal cracking risk of HPC through experiments and numerical simulations of a bridge pier cross section. Key findings include.

1) SF enhances early-age compressive and tensile strengths while slightly reducing total hydration heat. The ultimate degree of hydration increases linearly with SF replacement percentage as follows:

$$\alpha_u = \alpha_{u,0} + k_{SF}.p_{SF} = \alpha_{u,0} + 0.23p_{SF}. \quad (24)$$

2) SF00 and SF05 exhibited high thermal cracking risk, with thermal stress exceeding tensile strength between 48 and 90 h ($\eta > 1.0$).

3) SF10 and SF15 showed low cracking risk, as tensile stress remained below tensile strength for 7 d ($\eta < 1.0$).

4) Temperature differential (ΔT) decreased with higher SF content, but thermal stress trends varied due to creep behavior and changes in elastic modulus. SF05 had higher stress than SF00 despite a lower ΔT.

5) The reduction in cracking risk with SF replacement reflects a combined effect of tensile strength enhancement and reduced heat generation. While the present results suggest that strength development is more influential, the relative contributions were not quantitatively separated and should be further investigated.

From a practical standpoint, SF replacement at levels of 10%–15% is recommended as it provides sufficient thermal crack resistance during the critical early-age period while maintaining mechanical performance. Within this range, the results of this study justify 15% SF replacement as the optimal dosage for bridge pier applications. This offers valuable insights for designing durable and resilient HPC bridge structures, where early-age cracking is a significant concern.

Acknowledgements This research was funded by the University of Transport and Communications under grant number T2024-CT-003TĐ.

Competing interests The authors declare that they have no competing interests.

References

1. American Concrete Institute 207.1R-05. Guide to Mass Concrete. Farmington Hills, MI, 2005
2. ACI 207.2R-07. Report on Thermal and Volume Change Effects on Cracking of Mass Concrete. Farmington Hills, MI: American Concrete Institute, 2007
3. Nguyen C T, Do T A, Hoang T T, Tran T D. Evaluation of early-age cracking risk in mass concrete footings under different placement conditions. Journal of Construction Engineering, 2021, 36(1): 5–13
4. Lin Y, Chen H. Thermal analysis and adiabatic calorimetry for early-age concrete members. Journal of Thermal Analysis and Calorimetry, 2015, 122(2): 937–945
5. Nguyen-Ngoc L, Do T A, Hoang V H, Hoang T T, Tran T D. Equivalent convective heat transfer coefficient for boundary conditions in temperature prediction of early-age concrete elements using FD and PSO. KSCE Journal of Civil Engineering, 2023, 27(6): 2546–2558
6. Do T A, Ha L M, Nguyen Q T, Tran T D, Tham T Q. Evaluation of methods for analyzing early-age cracking risk in concrete walls of tunnel structures. Transport and Communications Science Journal, 2020, 71(7): 746–759
7. Viet H H, Anh T D, Duc T P. Utilizing artificial neural networks to anticipate early-age thermal parameters in concrete piers. Transport and Communications Science Journal, 2023, 74(4): 445–455
8. Ferraro C C. Determination of test methods for the prediction of the behavior of mass concrete. Dissertation for the Doctoral Degree. Gainesville, FL: University of Florida, 2009
9. Do T A, Nguyen T H, Vu T X, Hoang T T, Tran T D, Bui T T. Adiabatic temperature rise and thermal analysis of high-performance concrete bridge elements. In: Proceedings of ICSCEA 2019. Singapore: Springer Singapore, 2020, 413–423
10. Tuyet H T, Nam N H. Degree of hydration and strength development in high-strength concrete. Transport and Communications Science Journal, 2019, 70(2): 85–94
11. Do T A, Verdugo D, Tia M, Hoang T T. Effect of volume-to-surface area ratio and heat of hydration on early-age thermal behavior of precast concrete segmental box girders. Case Studies in Thermal Engineering, 2021, 28: 101448
12. Do T A, Tia M, Nguyen T H, Hoang T T, Tran T D. Assessment of Temperature Evolution and Early-Age Thermal Cracking Risk in Segmental High-Strength Concrete Box Girder Diaphragms. KSCE Journal of Civil Engineering, 2022, 26(1): 166–182
13. Li L, Dabarera A, Dao V. Evaluation of zero-stress temperature and cracking temperature of high performance concrete at early ages. Materials and Structures, 2022, 55(7): 181
14. Ruano G, Quintana V, La Scala A, Foti D. On the effect of thermal strains in slender prestressed concrete beams. Materials and Structures, 2025, 58(7): 244
15. Phan T N, Hosoda A, Tsujita Y, Shirakawa A. Numerical simulation for early-age cracking mitigation in durable RC deck slab on multiple span steel box girder bridges considering thermal and stepwise construction stresses. In: Proceedings of the International RILEM Conference on Synergising expertise towards sustainability and robustness of CBMs and concrete structures. Cham: Springer Nature Switzerland, 2023, 1093–1105
16. Tia M, Ferraro C C, Lawrence A, Smith S, Ochiai E. Development

of Design Parameters for Mass Concrete Using Finite Element Analysis. Florida Department of Transportation Final Report. 2010
17. Lawrence A M, Tia M, Ferraro C C, Bergin M. Effect of early age strength on cracking in mass concrete containing different supplementary cementitious materials: Experimental and finite-element investigation. Journal of Materials in Civil Engineering, 2012, 24(4): 362–372
18. Lin Y, Chen H L. Thermal analysis and adiabatic calorimetry for early-age concrete members. Journal of Thermal Analysis and Calorimetry, 2016, 124(1): 227–239
19. ACI 234R-06. Guide for the Use of Silica Fume in Concrete. Farmington Hills, MI: American Concrete Institute, 2006
20. Malhotra V M. Condensed silica fume in concrete. Boca Raton: CRC Press, 2018
21. Kurdowski W, Nocuń-Wczelik W. The tricalcium silicate hydration in the presence of active silica. Cement and Concrete Research, 1983, 13(3): 341–348
22. Cheng-yi H, Feldman R F. Hydration reactions in Portland cement-silica fume blends. Cement and Concrete Research, 1985, 15(4): 585–592
23. Kumar A, Roy D M. A Study of Silica-Fume-Modified Cements of Varied Fineness. Journal of the American Ceramic Society, 1984, 67(1): 61–64
24. Meland I. Influence of condensed silica fume and fly ash on the heat evolution in cement pastes. Special Publication, 1983, 79: 665–676
25. Shen D. Early-age Cracking Control on Modern Concrete. Singapore: Springer Nature Singapore, 2024, 143–157
26. Hamada H M, Abed F, Binti Katman H Y, Humada A M, Al Jawahery M S, Majdi A, Yousif S T, Thomas B S. Effect of silica fume on the properties of sustainable cement concrete. Journal of Materials Research and Technology, 2023, 24: 8887–8908
27. Singh A, Singh N. Mechanical properties of silica fume based concrete: A review. Materials Today: Proceedings, 2024
28. Shen D, Kang J, Jiao Y, Li M, Li C. Effects of different silica fume dosages on early-age behavior and cracking resistance of high strength concrete under restrained condition. Construction and Building Materials, 2020, 263: 120218
29. Xi J, Liu J, Yang K, Zhang S, Han F, Sha J, Zheng X. Role of silica fume on hydration and strength development of ultra-high performance concrete. Construction and Building Materials, 2022, 338: 127600
30. Smarzewski P. Mechanical and microstructural studies of high performance concrete with condensed silica fume. Applied Sciences, 2023, 13(4): 2510
31. Peknikova A, Jerabek J, Gandel R, Gabor R, Bilek V, Sucharda O. Physical–mechanical behavior of high-performance concrete and ordinary concrete with portland cement mixtures after exposure to selected durability tests including high thermal stress. Buildings, 2025, 15(7): 1029
32. ASTM C1240-15. Standard Specification for Silica Fume Used in Cementitious Mixtures. West Conshohocken, PA: ASTM International, 2015
33. ACI 211.4R-08. Guide for Selecting Proportions for High-Strength Concrete Using Portland Cement and Other Cementitious Materials. Farmington Hills, MI: American Concrete Institute, 2008
34. ASTM C39/C39M-01. Standard Test Method for Compressive Strength of Cylindrical Concrete Specimens. West Conshohocken, PA: ASTM International, 2001
35. ASTM C496/C496M-04. Standard Test Method for Splitting Tensile Strength of Cylindrical Concrete Specimens. West Conshohocken, PA: ASTM International, 2004
36. Gibbon G, Ballim Y, Grieve G. A low-cost, computer-controlled adiabatic calorimeter for determining the heat of hydration of concrete. Journal of Testing and Evaluation, 1997, 25(2): 261–266
37. Schindler A K, Folliard K J. Heat of hydration models for cementitious materials. ACI Materials Journal, 2005, 102(1): 24
38. Poole J L. Modeling Temperature Sensitivity and Heat Evolution of Concrete. Austin: The University of Texas at Austin, 2007
39. ASTM C531. Standard Test Method for the Coefficient of Thermal Expansion of Hydraulic Cement Concrete. West Conshohocken, PA: ASTM International, 2009
40. De Schutter G. Fundamental study of early age concrete behaviour as a basis for durable concrete structures. Materials and Structures, 2002, 35(1): 15–21
41. Fairbairn E M R, Azenha M. Thermal Cracking of Massive Concrete Structures. RILEM Technical Committee State-of-the-Art Report. 2019
42. ACI 209.2R-08. Guide for Modeling and Calculating Shrinkage and Creep in Hardened Concrete. Farmington Hills, MI: American Concrete Institute, 2008
43. Naik T R, Kraus R N, Kumar R. Influence of types of coarse aggregates on the coefficient of thermal expansion of concrete. Journal of Materials in Civil Engineering, 2011, 23(4): 467–472
44. Nguyen H T, Cosson B, Lacrampe M F, Do T A. Numerical simulation of reactive polymer flow during rotational molding using smoothed particle hydrodynamics method and experimental verification. International Journal of Material Forming, 2018, 11(4): 583–592
45. Do T A, Chen H L, Leon G, Nguyen T H. A combined finite difference and finite element model for temperature and stress predictions of cast-in-place cap beam on precast columns. Construction and Building Materials, 2019, 217: 172–184
46. Schindler A K, Frank McCullough B. Importance of concrete temperature control during concrete pavement construction in hot weather conditions. Transportation Research Record: Journal of the Transportation Research Board, 2002, 1813(1): 3–10
47. Kim S G. Effect of heat generation from cement hydration on mass concrete placement. Thesis for the Master's Degree. Ames: Iowa State University, 2010
48. Yikici T A, Chen H L. Numerical prediction model for temperature development in mass concrete structures. Transportation Research Record: Journal of the Transportation Research Board, 2015, 2508(1): 102–110
49. KCI 2003. Standard Specification for Concrete. Seoul: Korea Concrete Institute, 2003
50. Riding K A, Poole J L, Schindler A K, Juenger M C G, Folliard K J. Statistical determination of cracking probability for mass concrete. Journal of Materials in Civil Engineering, 2014, 26(9): 04014058
51. Kanda T, Momose H, Imamoto K, Mihashi H. Stochastic approach to shrinkage cracking control for reinforced concrete structural elements. Journal of Advanced Concrete Technology, 2008, 6(1): 121–133
52. Liu Y, Schindler A K. Finite-element modeling of early-age concrete stress development. Journal of Materials in Civil Engineering, 2020, 32(1): 04019338